Geopersia 2024, 14(2): 231-247
DOI: 10.22059/GEOPE.2024.354991.648702

RESEARCH PAPER

# Comparative Evaluation of Laboratory Permeability Measurement Approaches of a Carbonate Formation

**Jafar Vali [1,2], Farnusch Hajizadeh [3, *]**

[1] Department of Mining Engineering, Faculty of Engineering, Urmia University, Urmia, Iran
[2] Reservoir Rock and Fluids Research Group, Petroleum Engineering Department, Research Institute of Petroleum Industry, Tehran, Iran
[3] Department of Mining Engineering, Faculty of Engineering, Urmia University, Urmia, Iran

Received: 06 February 2023, Revised: 14 February 2024, Accepted: 27 February 2024


**Abstract**
As the phenomenon of gas slippage in rock pores is considered, the relationships between liquid equivalent permeability and absolute air permeability of 171 core plug samples of a carbonate reservoir from Dalan Formation were evaluated. Conventional absolute gas permeability measurement is generally much cheaper and faster than liquid permeability measurement. In this study, a comparative laboratory investigation of the permeability determination of carbonate rocks is represented. Air permeability, Klinkenberg corrected, and absolute water permeability experiments were performed. The gas permeability measurements at steady-state, unsteady-state, atmospheric flow, and back pressure flow modes were also examined in this research. The samples were divided into two permeability ranges of 0.1 to 1 mD and 1 to 1000 mD. The exponential relationship provided the best fit between absolute water, Klinkenberg, and air permeability values. It is best to use the constant back pressure method for samples with higher permeability to avoid errors in calculating the Klinkenberg factor, b. The Klinkenberg permeability was up to 7.2 times larger than the absolute water permeability due to the polar nature of water molecules. These results are helpful in providing a better basis for the prediction of Klinkenberg and water permeability values for this formation and similar carbonate reservoirs than the available correlations.

**Keywords:** Klinkenberg, Permeability, Slippage, Carbonate, Dalan Formation.

## Introduction

Significant gas reserves have been discovered in the Dalan Formation of the Qatar-South Fars arch, mainly called the South Pars gas field (Fotovat et al., 2011). A comprehensive assessment of petrophysical properties and their inter-relationships of carbonate rocks in Dalan Formation is needed for a sophisticated understanding of these giant carbonate reservoirs.

Permeability is an essential property of a porous medium, which it indicates its ability to pass a fluid.

Furthermore, air permeability is one of the basic petrophysical properties of hydrocarbon reservoir formations, routinely it is measured on subsurface core samples at laboratory conditions at a low cost. The basis for measuring a core sample's permeability is generating a constant pressure gradient under steady-state flow conditions, which it is proportional to the flow velocity formulated by Darcy's law (Equation 1). The Darcy relation is acceptable for a wide range of flow velocities. Furthermore, for low permeability core samples (less than 0.1

* Corresponding author e-mail: F.Hajizadeh@urmia.ac.ir

mD), it is not easily possible to achieve a steady flow in an acceptable time for testing, mainly when a liquid is used as a fluid to determine permeability. Therefore, the use of gas in determining permeability is recommended on both economic and time scales. However, factors such as gas slippage and flow inertia are two important factors in creating error and deviation from the Darcy equation in determining permeability (McPhee et al., 2015), which it causes nonlinearity and deviation from the Darcy formula (Galiuk & Delshad, 2013).

$$v = \frac{k}{\mu}\frac{d_p}{d_L} \qquad \text{(Equation 1)}$$

where, $v$ is the apparent fluid flowing velocity (cm/sec), $k$ is proportionality constant or permeability (Darcy), $\mu$ is the viscosity of the flowing fluid (cP), and $\frac{d_p}{d_L}$ is pressure drop per unit length (atm/cm).

When the average size of the radii of the throat of the rock is close to the average free path of the gas molecules, it causes the gas molecules to accelerate or slip in contact with the rock surface (Kazemi & Takbiri-Borujeni, 2016). The results which had been obtained by Nazari-Moghaddam & Jamiolahmady (2016) showed that slip coefficients in porous media are higher than those in non-porous systems. The molecular weight of the gas, the size of the gas passageways through the rock pores, and the gas pressure are the most important factors affecting the slippage of gases is. The lower the molecular weight of the gases, the greater the amount of slip of the gases is (Klinkenberg, 1941). Also, the smaller the size of the gas passage is, the greater the effect of gas slippage is.

The phenomenon of slipping in gases is inversely related to the fluid flow pressure. The first study of the effects of gas slippage in a porous medium was carried out by Klinkenberg (1941). It was shown by him that the measured gas permeability was a function of the mean pressure (average of upstream and downstream gas pressures, $P_m$). In his definitive manuscript, it was shown by him that by taking several measurements of gas permeability over a range of pore pressures and extrapolating the regressed data to infinite mean pressure, the core permeability approaches to an inert liquid permeability ($K_L$) (McPhee et al., 2015).

$$K = K_L(1 + \frac{b}{P_m}) \qquad \text{(Equation 2)}$$

The intercept of the linear fit curve of measured permeability at different mean pressures with cross line is equivalent to liquid permeability ($K_L$) or Klinkenberg corrected permeability, and the slope of this line is the gas slippage coefficient ($b$).

$K_L$ is gas permeability at an infinitely mean pressure, which it is theoretically equal to liquid permeability. Laboratories can use different gases and measure gas permeability at different mean pressures. Hence, the $K_L$ at infinite mean pressure will always be the same. Gas permeability measurements are based on two distinct approaches steady-state and unsteady-state flow conditions. Rushing et al. (2004) compared Klinkenberg's corrected permeability measurements in tight gas sands using steady-state and unsteady-state techniques. Their study showed that the unsteady-state technique consistently overestimates the steady-state permeability, even when the steady-state measurement corrected for gas slippage and inertial effects. It has also been shown by them that the results are similar for constant backpressure and constant mass flow rate test conditions. Jones (1972) investigated the relationship between Klinkenberg slip factor b and estimated $K_L$ for about 100 core samples, finding that the logarithm of b decreases linearly with an increase in the logarithm of $K_L$.

Conventionally, $K_L$ is determined on a limited number of subsurface core samples of a specific reservoir formation to reduce the cost and time of a core analysis project. Hence, mathematically developed equations predict $K_L$ from routine gas permeability data set. However, since there is a significant discrepancy between $K_L$ and absolute brine permeability

($K_W$), $K_L$ is not directly embedded into the reservoir dynamic model. The $K_W$ data set is generally limited to a much smaller quantity of selected samples for special core analysis (SCAL) experiments. Hence, some empirical equations were developed to relate $K_L$ with $K_W$. An empirical correlation for liquid and gas permeability measurements obtained for a suite of Permo-Triassic sandstones and shales from the sandstone group of northern England was presented by Bloomfield & Williams (1995). Moreover, liquid permeability tests were performed using synthetic brines and deionized water. The gas permeability test, Nitrogen was used as the permeant. $K_L$/kg ratio has been obtained in the range of 0.03 to 0.9. Li et al. (2009) presented an experimental method has to study the slip effect in gas permeability measurements for low permeability cores by applying a backpressure at the outlet of test samples. The non-slip gas permeability can be determined without using the Klinkenberg correlation with backpressures equal to or greater than the minimum backpressure.

In a research, the permeabilities of nitrogen gas and water on the same core samples have been measured by Tanikawa & Shimamoto (2009). The intrinsic permeability of sedimentary rocks from the Western Foothills of Taiwan was measured using nitrogen gas and distilled water as pore fluids, during several effective-pressure cycling tests at room temperature. The observed difference in gas and water permeability was analyzed regarding the Klinkenberg effect. Their experimental results have shown that gas permeability is larger than water permeability by one to several times order of magnitude. Thus, water permeability can be estimated from gas permeability. They attributed the higher estimate of Klinkenberg permeability to factors such as the adhesion of water molecules to crystalline surfaces and the reaction of water with clay.

Some exponential equations for predicting the equivalent liquid permeability of carbonate core samples of Southwest Iran from the absolute air permeability (Equation 3) were obtained by Galiuk & Delshad (2013). A smaller correlation coefficient for samples with permeability of less than 1 mD has been observed by them. In addition, previous studies were performed on a limited range of permeability. The gas permeability of sedimentary rocks can be larger than water permeability several times to one order of magnitude (Tanikawa & Shimamoto, 2009).

$K_l = 0.5577K_{air}^{1.0616}$ ($R^2$>0.936) (Equation 3)

Also, the correlation between liquid and gas permeability for the pure dolomite samples of a formation in Poland has been studied by Wojnarowski et al. (2018). The results showed that Klinkenberg permeability overestimates water permeability and the observed difference is in the range of 11–24%. They inferred that due to the water's polar nature, the hydrogen bonds are formed with neighboring molecules and cause high surface tension and capillary forces.

Furthermore, in 2021 Ahmad et al. (2021) have studied the theoretical concept that the water permeability is lower than $K_L$, and experimental hints have indicated that $K_L$ and the water permeability are different. Thus, a series of gas and water permeability measurements was conducted on eight carbonate core plug samples from Sarawak, Malaysia, to develop a correlation between both permeability values. The new $K_L$ versus $k_W$ correlation proved the differences between both permeability values for all samples, which it proved the migration of fines and clay particles that blocked the pore throats, thus reducing $k_W$ values.

Furthermore, in 2022, the clayey-silt marine sediments of the south China sea were studied by Lei et al. (2022) to evaluate the effects of hydrate saturation, effective stress, pore pressure, and osmotic pressure on the gas flow patterns. The results indicated that when the hydrate saturation increased the gas flow changes from viscous flow to slip flow, and the gas slippage effect gets more and more pronounced with an increase in hydrate saturation. Elevated pore pressure led to a small decrease in gas permeability, but it did not alter the flow pattern of fluid flow in the marine sediment.

Although some researchers (e.g. (Kadkhodaie et al., 2011; Sfidari et al., 2012; Rastegarnia & Kadkhodaie-Ilkhchi, 2013) presented neural network approaches to predict permeability

from conventional well logs, empirical equations generated from direct measurements are more desirable. In this research, correlations that are applicable to other carbonate reservoirs in the Middle East with some minor deviations have been obtained.

*Geological Settings of the Studied Carbonate Formation*

The Upper Dalan and Kangan Formations (Khuff-equivalent) with Permian-Triassic age host the World's largest gas reserves in the Persian Gulf (Figure 1). This carbonate succession is a heterogeneous reservoir because of its geological and petrophysical characteristics (Rahimpour-Bonab et al., 2010; Tavakoli et al., 2011; Tavakoli, 2021). The central part of the Persian Gulf as a part of the NE margin of the Arabian Plate experienced a complex geological–structural evolution from the Pre-Cambrian to recent times. The morphology of this area was highly affected by the Qatar-Fars Arc, as a regional SW-NE structure in the central Persian Gulf (Martin, 2001). It is a very large (more than 100 km wide and 300 km long) and gentle anticline (Insalaco et al., 2006).

At the late Permian, a marine transgression along with the opening of the Neo-Tethys Ocean resulted in the development of a homoclinic ramp on the passive NE margin of the Arabian Plate (Martin, 2001). Consequently, thick carbonate–evaporate sequences (Dalan and Kangan Formations) were deposited on these platforms, during the late Permian to early Triassic (Insalaco et al. 2006; Martin 2001). The lower interval of these deposits, called the Dalan Formation is stratigraphically subdivided into three members including the lower Dalan, the Nar evaporate, and the upper Dalan (Mazaheri-Johari & Ghasemi-Nejad, 2017). This formation is overlain by the Early Triassic Kangan Formation along the Permian–Triassic boundary unconformity (Szabo & Kheradpir, 1978).

According to the lithological properties, the upper Dalan succession was divided into two reservoir units, K3 and K4 (Insalaco et al., 2006). Accordingly, the K4 and K3 units were mainly composed of limestone to dolomitic limestone (K4) and dolostone to anhydritic dolostone (K3) precipitated in a shallow marine ramp setting. Due to the reservoir importance of this carbonate sequence, several researchers have focused their studies on its sedimentological and reservoir aspects (Insalaco et al., 2006; Rahimpour-Bonab et al., 2010; Tavakoli et al., 2011; Mehrabi et al., 2019; Mehrabi et al., 2021; Tavakoli, 2021; Tavoosi-Iraj et al., 2021).

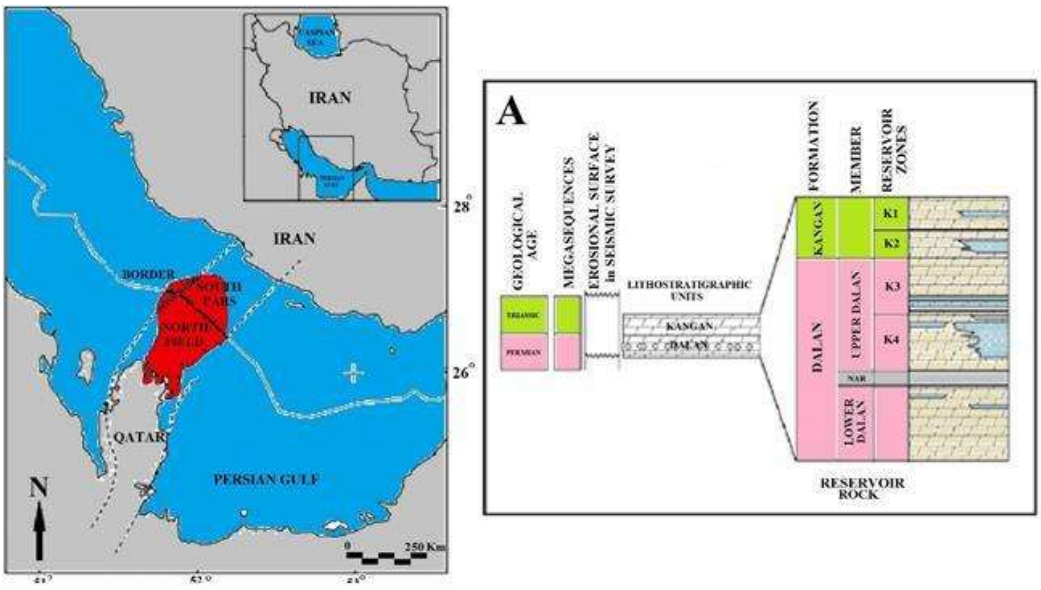


**Figure 1.** Location map of the study Gas Field, South of Iran. A: Generalized stratigraphy of the upper Permian–lower Triassic at the South Pars (Aghanabati et al., 2014; Fotovat et al., 2011)

Based on the studies, the reservoir quality of this highly heterogeneous reservoir sequence is controlled by facies parameters (e.g. texture, grain size) and especially by various diagenesis processes (e.g. dolomitization, anhydrite precipitation, dissolution, and compaction). Geological parameters, especially the diagenesis processes affecting the Dalan Formation, have caused the formation and expansion of various types of porosity in this formation ( Rahimpour-Bonab et al., 2010; Mehrabi et al., 2019). Porosity with different genesis, size, and connectivity has caused the relationship between porosity and permeability to be very complicated (Kadkhodaie-Ilkhchi A. & Kadkhodaie-Ilkhchi R., 2018; Kadkhodaie et al., 2019; Mehrabi et al., 2019). Numerous studies conducted on this formation have shown that diagenesis processes such as compaction, calcite cementation, anhydrite precipitation, dissolution, and dolomitization have played the most important role in controlling reservoir properties. In Table 1 and Figure 2, the variety of facies and diagenesis features that caused the extremely high heterogeneity of reservoir properties in this formation are depicted.

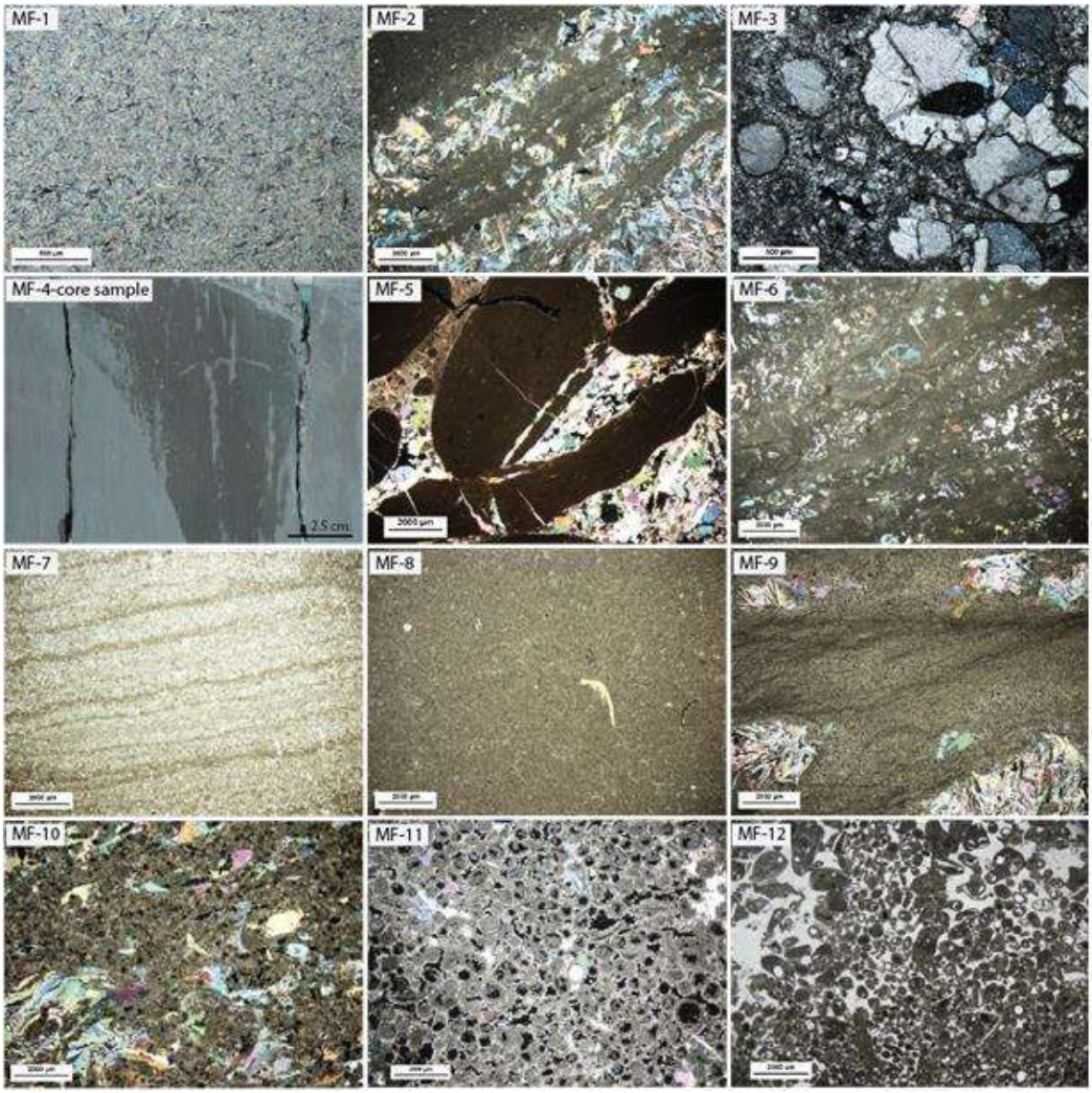


**Figure 2.** Thin section photomicrographs from various microfacies of the Dalan Formation in the studied well. Diagenetic processes like calcite cementation (MF-3), anhydrite plugging (MF-10, 11, 12) and dissolution (MF-11) can be observed. MF-4 was shown in the core sample (modified from Moradpour et al. (2010))

**Table 1.** microfacies descriptions and their depositional setting of Dalan Formation.

| Facies Belt | Name | Description | Depositional setting |
|---|---|---|---|
| Sabkha / Supra tidal | MF1 | Massive to laminated Anhydrite (>10 cm in thickness, >70% anhydrite). Syn-depositional. | Evaporitic flats or saltern (Supratidal to intertidal setting) |
| | MF2 | Mudstone to Wackestone (often laminated) with anhydrite (greater than 20%, nodular or laminated). Syn-depositional or replacive anhydrite. | Evaporitic flats or saltern (Supratidal to intertidal setting) and early diagenetic replacement; Karstification and brecciation are common. |
| Tidal Flat | MF3 | Coarse to Very coarse-grained Packstone to Grainstone with pebbles and lithoclasts (Intra-formational Conglomerate). | High-energy upper intertidal settings (tidal channels, flood and ebb tidal deltas, upper shoreface). |
| | MF4 | Green to grey Shaly Mudstone (often dolomitized mudstone) laminated, liquefaction features | Restricted tidal flat environment (upper intertidal to intertidal mudflats) |
| | MF5 | Very fine to medium sand-grained Oolitic/Peloidal Packstone to Grainstone with anhydrite cement, small reworked micritic lithoclasts and occasionally oncoids | High-energy upper intertidal settings, represent marine pebbly beach-type environments, storm lag sheets or the bases of channel lags. |
| | MF6 | Thin laminated light brown to cream Mudstone to Wackestone (often dolomitic), often associated with anhydrite, teepee structures and microbial mat laminations, desiccation cracks, fenestral fabric, minor exposure surface and occasional burrows. | Non-saline low energy Intertidal-mudflats and microbial mudflats |
| Lagoon | MF7 | Stromatolite Boundstone, it is observed as cream to grey color laminated to thinly-bedded microbial Mudstone to Wackestone. | Intertidal to Lower Intertidal Setting |
| | MF8 | Structureless light brown to cream Mudstone to Packstone (often dolomitic) | Lagoon |
| | MF9 | Structureless light brown to cream mudstone to Wackestone (often dolomitic), with dark grey mottled texture and anhydrite (occasional monospecific bioturbation); | Hypersaline lagoon settings |
| Shoal | MF10 | Fine to coarse sand-grained Peloidal/Ooidal bioclastic Packstone to Grainstone; sometimes with intercalation of very fine-grained sand to silt grade, often laminated. | Leeward shoals with algae, mollusc and gastropod, associated with subtidal setting microfacies. |
| | MF11 | Medium to coarse-grained Oolitic/Ooidal/bioclastic Grainstone with minor amount of oncoids. | Center Shoal (High energy Oolitic to Ooidal Bioclastic shoal belts) |
| | MF12 | Coarse to Very coarse-grained Ooidal/Bioclastic/oncoidal Grainstone: | High energy Seaward Shoal setting |

Interconnected porosities such as intergranular and intercrystalline types and isolated porosities such as moldic and vuggy types have played different roles in increasing the permeability of this formation so that, unlike the first type, the second type of porosities have little role in increasing the permeability and production potential.

## Methodology

Cylindrical samples (plugs) of 1.5″ diameter and 2″ long were prepared from subsurface whole cores of Dalan carbonate formation in Southwest Iran. The total number of 171 core plug samples drilled parallel to the reservoir layers, excluding highly vuggy or fractured ones, was selected by visual inspection. To remove the in-situ hydrocarbons, the samples were washed in a Soxhlet extraction apparatus with adequate fractions of toluene and methanol. The samples were then dried in a conventional oven for 24 hours. The sample porosity was measured by Core Lab Ultra-porosimeter by helium expansion at ambient conditions.

*Steady-state gas permeability measurement*

The absolute gas permeability was measured by an Ultra-Permeameter apparatus from CoreLab. Moreover, Nitrogen (99.9% purity) was used as the inert gas. Furthermore, the measurement approach is based on the Darcy law and applies a gas pressure difference or constant gas flow rate on the sample. The experiment was performed at a hydrostatic confining stress of 400 psig. The $K_L$ at steady-state flow conditions requires the measurement of gas permeability at three or more different mean pressures (average of upstream and downstream pressure). In a diagram similar to Figure 3, the values of absolute permeability to air at different mean pressures are plotted. The $K_L$ is obtained by extending the fitted trend line to the intercept point with the vertical axis, the point at which the average pressure of the gas is infinite.

Klinkenberg measurement can be made at atmospheric flow mode, backpressure flow mode, under either constant differential pressure, or constant mass flow rate. In atmospheric flow measurements, the gas leaving the core flows directly into the atmosphere. The mean pressure and flow rate can only be controlled by adjusting the injection flow rate. In backpressure flow mode, a pore pressure is created at the outlet of the sample. Pressure and flow rate can be controlled independently. In constant differential pressure mode, the pressure drop across the core remains constant. 19 core samples underwent $K_L$ experiment by direct flow to the atmosphere, and 31 samples at backpressure flow mode. Table 2 shows the frequency of 171 samples in terms of percentage in the range of porosity and Klinkenberg permeability. The highest frequency (25.7%) of samples is related to the porosity range of 15% to 20%.

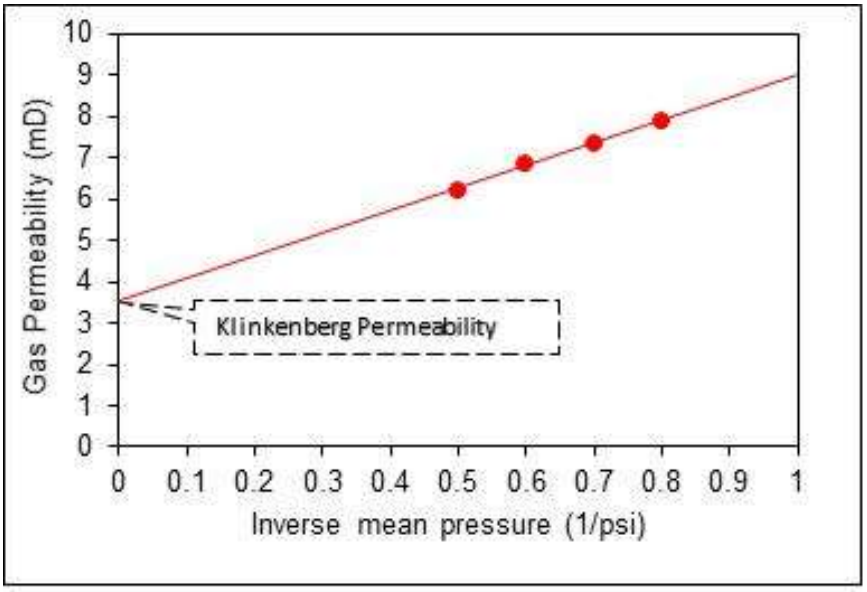


**Figure 3.** Effect of gas pressure on measured gas permeability, a Klinkenberg plot (Klinkenberg, 1941)

**Table 2.** 171 samples in terms of percentage in the range of porosity and Klinkenberg permeability.

| Porosity range (%) | Klinkenberg Permeability range (mD) | Quantity of Selected samples | percentage of Selected samples |
|---|---|---|---|
| 0-5 | - | 0 | 0.0 |
| 5-10 | 0.06 - 20.10 | 22 | 12.9 |
| 10-15 | 0.10 - 395.10 | 41 | 24.0 |
| 15-20 | 0.245 - 160.81 | 44 | 25.7 |
| 20-25 | 0.07 - 534.15 | 27 | 15.8 |
| 25-30 | 0.13 - 249.22 | 29 | 17.0 |
| 30-35 | 0.11 - 113.26 | 7 | 4.1 |
| 35-40 | 0.07 | 1 | 0.6 |
| Total: | | 171 | 100.0 |

*Unsteady-state gas permeability measurement*

Additionally, the Klinkenberg permeability of the samples was measured by the unsteady-state method at a hydrostatic confining stress of 400 psi. For this purpose, the CMS-300 apparatus made by CoreLab was employed. The apparatus can measure both porosity and $K_L$ at different mean pressure steps using a pressure pulse decay procedure. Pulse decay techniques were developed by utilizing a differential pressure between the upstream and downstream of a confined porous medium. More detail about the applied approach was explained in other manuscripts (Sharifigaliuk et al., 2023).

*Absolute water permeability measurement*

The clean samples were saturated with formation brine of 186000 ppm salinity in an evacuated tight vessel for absolute water permeability measurement. The plug samples were submerged in the brine for two weeks to attain ionic equilibrium conditions (Behin & Sharifi-Galiuk, 2010; Sharifi-Galiuk et al., 2012; Khosravi et al., 2022). The saturated sample was loaded into a core holder under 400 psi hydrostatic confining pressure. Brine was injected into the core plug using a high-pressure pump connected to the brine accumulator. Different applied flow rates and maintained differential pressures were recorded, and the absolute water permeability was directly calculated from the Darcy equation. Multi-rate tests are preferred as this minimizes the impact of pressure transducer error on permeability derived from single-rate analysis.

## Results and Discussion

The measured Klinkenberg permeability of all the samples was plotted against their porosity in a semi-log plot (Figure 4). No logical relationship was observed between the corrected Klinkenberg permeability and the porosity of the samples. It is inferred that there is a high diversity in the petrophysical properties of studied samples due to the highly heterogeneous texture and structure of these carbonate rocks, even in a specific formation. Therefore, it was impossible to classify the samples based on their porosity-permeability characteristics. Jamal-Mustafa et al. (2020) proposed some power law relationships for carbonate rocks in some other regions of the Middle East. However, the scattered porosity-permeability data set (Figure 4) shows a substantial structural heterogeneity and pore anisotropy in Dalan Formation.

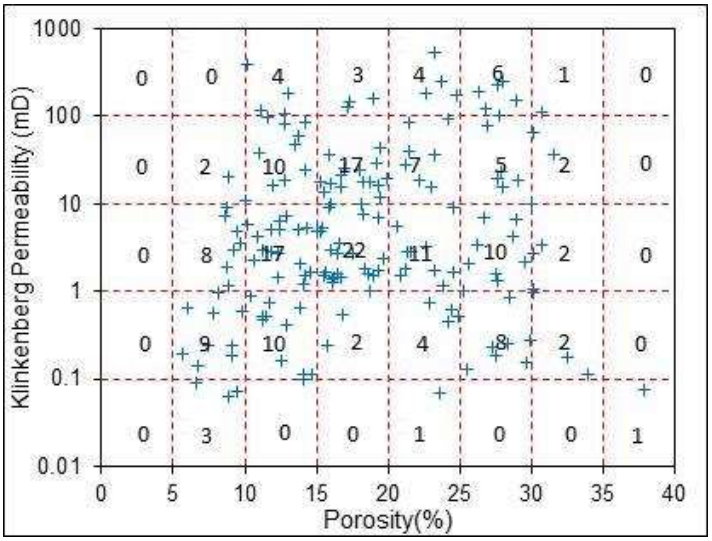


**Figure 4.** Porosity - permeability network and data diagram of 171 plug samples in this study

*Empirical $K_L$ versus $K_{air}$ relations*

By examining and analyzing the whole $K_L$ results obtained from laboratory data of carbonate samples of Dalan formation, an experimental model of $K_L$ versus $K_{air}$ in the logarithmic diagram was achieved (Figure 5). The data dispersion showed two permeability ranges of 0.1 to 1 and 1 to 1000 mD. The exponential functions have the best fit on the dataset (Equations 4 and 5). As observed in Figure 5, in the low permeability range (below 1 mD), the reduction of Klinkenberg permeability is greater than the permeability values higher than 1 mD. With these experimental correlations, the amount of $K_L$ in other zones of Dalan and nearby formations can be predicted in the range of 0.1 to 1000 mD without direct instrumental measurements.
Permeability ranges from 0.1 to 1 mD, and the average error rate in this range is 9.5%:

$K_L = 0.504{K_{air}}^{1.06}$ ($R^2$=0.89) (Equation 4)

Permeability ranges from 1 to 1000.0 mD, and the average error rate in this range is 5.9%:

$K_L = 0.619{K_{air}}^{1.07}$ ($R^2$=0.99) (Equation 5)

The samples with permeability less than 1 mD are in the range of tight rocks of hydrocarbon reservoirs in terms of rock texture and pore size. Hence, their laboratory measurement by devices faces the error of accurately determining the flow rate. Therefore, it results in more errors in the experimental models.

In Figure 6, the Klinkenberg factor, *b* versus Klinkenberg permeability was shown for selected samples and compared with the Jones, 1972 model. The Jones, 1972 model underestimates the predicted *b* values of this study. The amount of this factor decreased with an increase in permeability. The crucial assumption that the *b* factor is constant, and independent of mean pressure may not be valid for gas flow through higher permeability porous media at higher mean pressures. As shown in Figure 6, Klinkenberg factor, *b*, for samples of higher than 10 mD permeability is more dispersed. And, *b* for samples of less than 10 mD permeability is more compatible with the Jones, 1972 model.

It has been observed by Rushing et al. (2004) that the Klinkenberg factor, *b*, obtained with helium is higher than that of nitrogen gas in very tight sand samples with very low permeability. Similarly, for a wider range of selected carbonate samples, the same results have been obtained. In Figure 7, the *b* factor is much higher for samples measured with helium gas, which it is due to the lower molecular weight of helium than nitrogen. However, the *b* factor for samples measured by nitrogen gas is more compatible with the Jones, 1972 model.

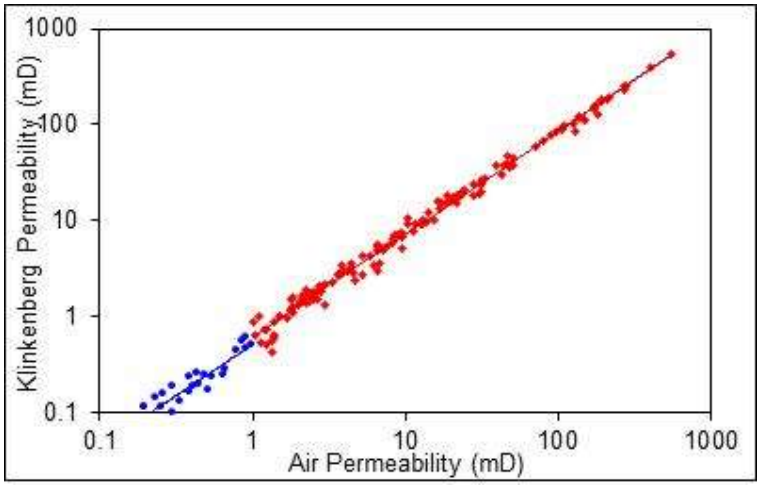


**Figure 1.** laboratory Klinkenberg permeability data measured versus air permeability. In the low permeability range (less than 1 mD), the decrease in Klinkenberg permeability is greater than in the higher permeability range

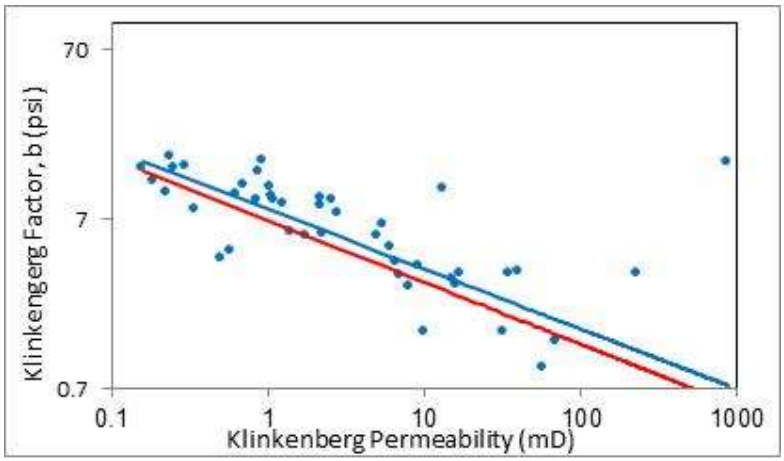


**Figure 2.** Klinkenberg factor, *b* versus Klinkenberg permeability of selected samples (blue points) and in comparison with Jones, 1972 model (red line)

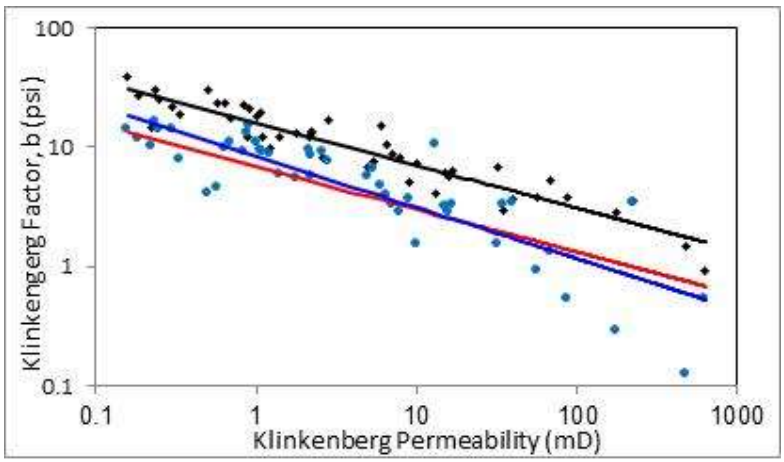


**Figure 3.** Klinkenberg factor, *b* (psi) versus Klinkenberg permeability (mD) by Helium gas (black points) and Nitrogen gas (blue points) injection in selected samples and comparison with Jones 1972 model (red line), for selected samples.

*Steady-state vs. unsteady-state gas permeability measurement*

Furthermore, Rushing et al. (2004) showed that the unsteady-state technique consistently overestimates the steady-state permeability, even when the steady-state measurements corrected for gas slippage and inertial effects. In an effort of measuring the Klinkenberg permeability of 47 selected samples by both unsteady-state and steady-state methods, $K_L$ was obtained more than twice higher for low permeability samples by unsteady-state technique (as seen in Figure 8).

*Correlation of absolute water permeability and $K_L$*

In 2009, the permeability of dry and water-saturated dolomite sedimentary rocks has been compared by Tanikawa & Shimamoto (2009). It was observed that gas permeability is more considerable than water permeability. However, water permeability can be estimated from the gas permeability. The Klinkenberg permeability of pure dolomite samples overestimated the water permeability, as a result of the water polar nature. Also the migration of fines and clay particles, blocking the pore throats, hence, reducing $k_W$ values has been notified by them. In our study on 37 selected carbonate samples, the nitrogen gas permeability was 1.3 to 10 times larger than absolute water permeability. Similarly, the Klinkenberg Permeability was 1.1 to 7.2 times larger than that of water on the same samples as a result of the water's polar nature. In Figure 9, the relationship between water permeability and air/Klinkenberg permeability is shown. Fortunately, the measured values are correlatable and water permeability of carbonate samples of this formation can be predicted with high accuracy (Equations for Figure 9 in Table 3).

*$K_L$ measurement at backpressure mode*

Applying backpressure at the outlet of core samples during gas permeability measurement offers several advantages. Firstly, the control of differential pressure and flow rate is improved. The range of mean pressure is also extended, yielding a less tenuous extrapolation to infinite mean pressure. In addition, the gas flow is restricted to the Darcy regime, even at relatively high mean pressures. Figures 10 and 11 show the Klinkenberg factor, *b* versus Klinkenberg permeability and average pressure in the backpressure test method for selected samples. This test is typically done for high gas permeability values and lower differential pressure, whereas, the gas flow must be restricted to the Darcy regime.

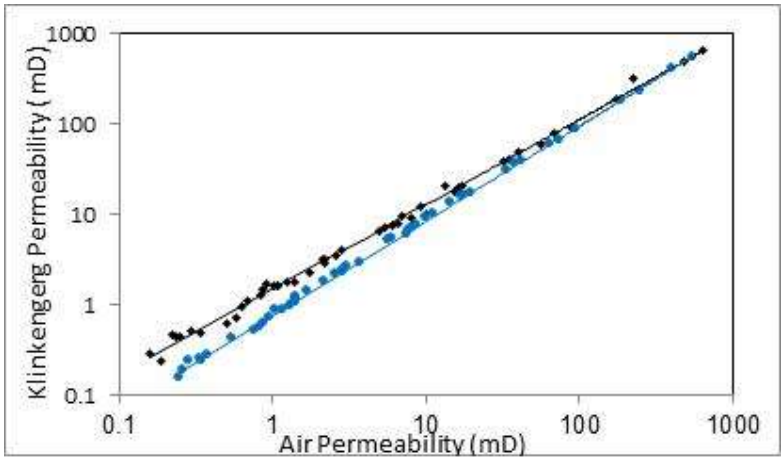


**Figure 4.** Klinkenberg permeability ($K_L$) versus Air Permeability by steady-state (blue points) and unsteady-state (black points) methods for selected samples

**Table 3.** The experimental formulas developed in this study based on the measured dataset

| Figure number | Parameter | Quantity of selected samples | Measurement/ prediction range | Unit | Formula | Regression coefficient ($R^2$) |
|---|---|---|---|---|---|---|
| 4 | Klinkenberg permeability, steady-state condition | 31 | 0.1-1 | mD | $K_L = 0.37\ K_{air}^{0.87}$ | 0.78 |
| 4 | Klinkenberg permeability, steady-state condition | 144 | 1-1000 | mD | $K_L = 0.60\ K_{air}^{1.07}$ | 0.98 |
| 5 | Laboratory measurement of Klinkenberg factor, (*b*) versus Klinkenberg permeability, unsteady-state condition | 50 | 0.1-1000 | psi | $b_{lab} = 8.04\ K_L^{-0.354}$ | 0.52 |
| 6 | Laboratory measurement of Klinkenberg factor, (*b*) by Helium gas, unsteady-state condition | 45 | 0.1-1000 | psi | $b_{(by\ Helium)} = 16.14\ K_{L\ (by\ Helium)}^{-0.36}$ | 0.82 |
| 6 | Laboratory measurement of Klinkenberg factor, (*b*) by Nitrogen gas, steady-state condition | 45 | 0.1-1000 | psi | $b_{(by\ Nitrogen)} = 8.38\ K_{L\ (by\ Nitrogen)}^{-0.43}$ | 0.65 |
| 7 | Laboratory measurement of Klinkenberg permeability in steady-state condition | 47 | 0.1-1000 | mD | $K_{L\ (Steady\text{-}state\ Method)} = 1.48\ K_{air\ (Steady\text{-}state\ Method)}^{0.94}$ | 0.99 |
| 7 | Laboratory measurement of Klinkenberg permeability in unsteady-state condition | 47 | 0.1-1000 | mD | $K_{L\ (Unsteady\text{-}state\ Method)} = 0.76\ K_{air\ (Unsteady\text{-}state\ Method)}^{1.05}$ | 0.99 |
| 8 | Laboratory measurement of water permeability versus Air permeability | 35 | 0.1-1000 | mD | $K_W = 0.29\ K_{air}^{1.07}$ | 0.93 |
| 8 | Laboratory measurement of water permeability versus Klinkenberg permeability | 35 | 0.1-1000 | mD | $K_W = 0.45\ K_L^{1.05}$ | 0.97 |
| 9 | Laboratory measurement of Klinkenberg factor, (*b*) by constant back pressure test, steady-state condition | 19 | 1-100 | psi | $b = 65.27\ K_L^{-0.25}$ | 0.79 |
| 10 | Laboratory measurement of Klinkenberg factor, (*b*) by constant backpressure test, steady-state condition | 19 | 0-100 | psi | $b = 22.82\ \Delta P^{0.31}$ | 0.63 |
| 11 | Laboratory measurement of Klinkenberg factor, (*b*) by constant mass flow rate test, steady-state condition | 19 | 0.1-1000 | mD | $b = 8.69\ K_L^{-0.32}$ | 0.79 |
| 12 | Laboratory measurement of Klinkenberg factor, *b* (psi) versus average differential pressure (psi) by constant mass flow rate test, steady-state condition | 19 | 0-40 | psi | $b = 0.52\ \Delta P^{0.89}$ | 0.55 |

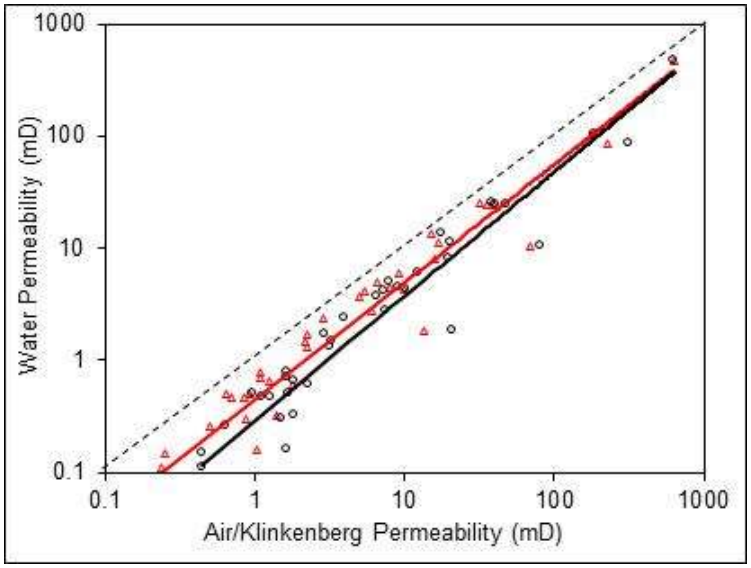


**Figure 9.** Water permeability ($K_W$) versus Air Permeability (black points) and Klinkenberg Permeability (red points) for selected samples

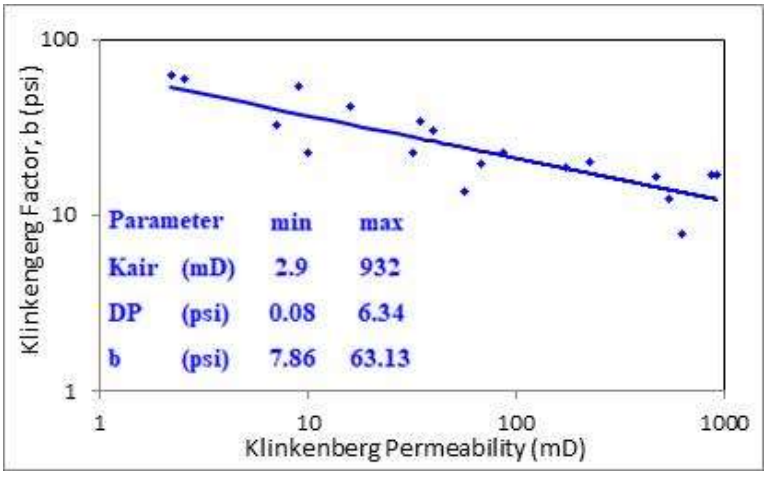


**Figure 5.** Klinkenberg factor, b (psi) versus Klinkenberg permeability (mD) by constant backpressure test for selected samples

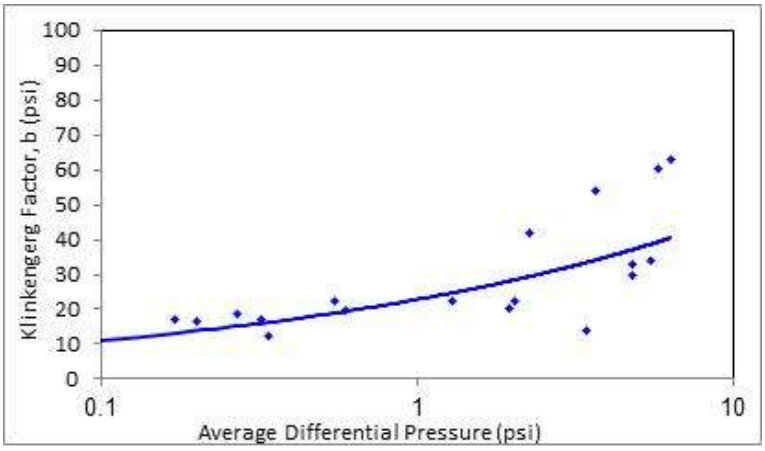


**Figure 6.** Klinkenberg factor, *b* (psi) versus average differential pressure (psi) by constant backpressure test for selected samples

Figures 12 and 13 show the Klinkenberg factor, *b* versus Klinkenberg permeability and average pressure in constant mass flow rate method for selected samples. This test is usually done for low gas permeability and higher differential pressure, whereas, in this test, the Klinkenberg factor, *b* is lower in high injection gas pressures. A summary of all parameters affecting the Klinkenberg permeability measurement and the resulting equations for the prediction of Klinkenberg and absolute water permeability has been shown in Table 3. The equations can be used for the rock samples from Dalan Formation in other wellbore and nearby carbonate formations. However, the formulas can be updated by embedding the new laboratory permeability measurements.

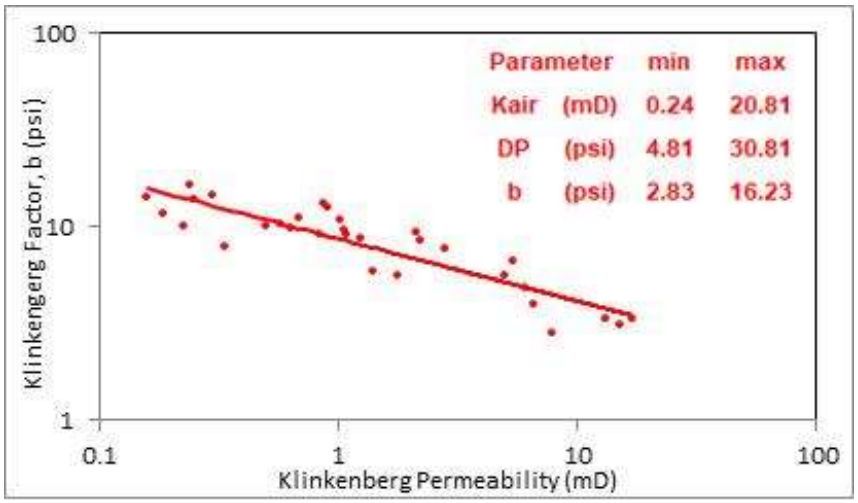


**Figure 7.** Klinkenberg factor, b (psi) versus Klinkenberg permeability (mD) by constant mass flow rate method for selected samples

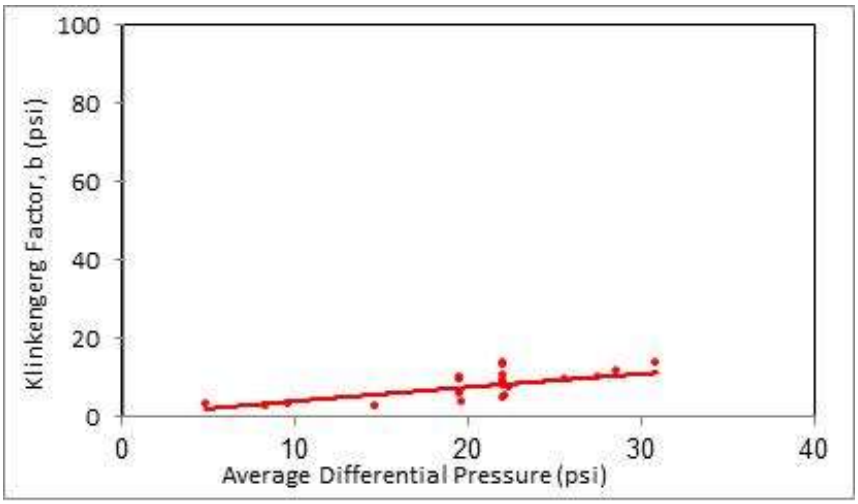


**Figure 8.** Klinkenberg factor, *b* (psi) versus average differential pressure (psi) by constant mass flow rate method for selected samples

## Conclusions

The following remarks and conclusions were derived from this study:

In the Dalan formation, no logical relationship between the Klinkenberg permeability and the porosity of the samples was observed, revealing high heterogeneity of this carbonate formation. Hence, it was impossible to classify the samples according to their porosity-

permeability values.

The exponential function ( $K_L = 0.504{K_{air}}^{1.06}$ ) best illustrates the $K_L$-Kair empirical relationship with the smallest error. However, the samples were differentiated to above and below permeability of 1 mD.

The Klinkenberg factor b, decreased with an increase in permeability. It has a higher dispersion for permeability values higher than 100 mD. In addition, this factor shows higher values than Jones, 1972 model.

In this study, the Klinkenberg factor, $b$ is much higher for samples measured with helium than with nitrogen. Unlike Klinkenberg permeability, the Klinkenberg factor depends on the type of gas. The permeability experiments measured with nitrogen are more compatible with the Jones, 1972 model.

Our study on 47 selected samples has shown the Klinkenberg permeability by unsteady-state measurement results about 2.5 times less than steady-state measurement data.

Nitrogen gas permeability was 1.3 to 10 times larger than absolute water permeability and also Klinkenberg Permeability was 1.1 to 7.2 times larger than that of water on the same samples, which it is due to the water's polar nature. However, water permeability versus air or Klinkenberg permeability in carbonate samples of this formation can be predicted with high accuracy.

**Acknowledgment**

This research was conducted at the Petroleum Engineering Research Division of the Research Institute of Petroleum Industry (RIPI), Tehran, Iran. The authors would like to thank the management and technicians of the Rock and Fluid Research Department for the experimental activities.

**Nomenclature**

**Parameters**

$b$, Gas slippage factor or Klinkenberg factor, Pa
CMS-300, Core measurement system apparatus
i, Intercept of curve in Darcy flow
$K_{air}$ or K, Absolute air permeability, $m^2$
$K_L$, $K_{liquid}$ or $K_{\infty}$, equivalent liquid or Klinkenberg permeability, $m^2$
$K_W$, Absolute water Permeability, $m^2$
m, Slope of curve in Darcy flow
P, Gas pressure, atm
$P_a$, Atmospheric pressure, atm
$P_m$, Mean pressure, atm
$d_p$: Differential pressure, atm
$d_L$: Sample length, m

**Greek letters**

β, compressibility factor
ρ, gas density, $kg/m^3$
μ, Fluid viscosity, cp
$v_x$, Darcy's velocity (or apparent fluid flowing velocity), cm/sec

**Subscripts**

L, Sample length, m
D, Sample diameter, m

## References

Aghanabati, A., Ghasemi Nejad, E., Mazaheri Johari, M., 2014. Biostratigraphy and Paleoenvironmental study of Permian-Triassic boundary in Dalan and Kangan formations, South Pars Gas Field, South West of Iran: Journal of Stratigraphy and Sedimentology Researches, 30 (2): 1-22.

Ahmad, I., Ahmad, M., and Ali, I., 2021. Klinkenberg-Corrected and Water Permeability Correlation for a Sarawak Carbonate Field: Fluids, 6 (10): 339.

Behin, R., and Sharifi Galiuk, H., 2010. Study of Two Phase Fluid Flow in Water Wet Reservoir Rocks by Using X-Ray In situ Saturation Monitoring: Journal of Petroleum Science and Technology, 1 (1): 15-23.

Bloomfield, J. P., Williams, A. T., 1995. An empirical liquid permeability—gas permeability correlation for use in aquifer properties studies: Quarterly Journal of Engineering Geology and Hydrogeology, 28 (2): S143-S150.

Fotovat, M., Hashemi Hosseini, G., Rahimpour-Bonab, H., 2011. Sedimentary environment of the Upper Dalan Member in the Qatar- Fars Arc and its eastern margins: South Pars and Salman fields: Journal of Stratigraphy and Sedimentology Researches, 27 (1): 115-136.

Galiuk, H. S., Delshad, Y. S., 2013. Klinkenberg Permeability Prediction by Using Absolute Gas Permeability in Carbonate Hydrocarbon Reservoir Rocks of South-West of Iran: Iranian Journal of Petroleum Geology, 3 (4):1-10.

Insalaco, E., Virgone, A., Courme, B., Gaillot, J., Kamali, M., Moallemi, A., Lotfpour, M., Monibi, S., 2006. Upper Dalan Member and Kangan Formation between the Zagros Mountains and offshore Fars, Iran: depositional system, biostratigraphy and stratigraphic architecture: GeoArabia, 11 (2): 75-176.

JamalMustafa, S., Rashid, F., Ismail, K. M., 2020. Liquid and Gas Corrected Permeability Correlation for Heterogeneous Carbonate Reservoir Rocks: Kurdistan Journal of Applied Research (KJAR), 5:2.

Jones, S. C., 1972. A Rapid Accurate Unsteady-State Klinkenberg Permeameter: Society of Petroleum Engineers Journal, 12: 383-397.

Kadkhodaie-Ilkhchi, A., and Kadkhodaie-Ilkhchi, R., 2018. A Review of Reservoir Rock Typing Methods in Carbonate Reservoirs: Relation between Geological, Seismic, and Reservoir Rock Types: Iranian Journal of Oil and Gas Science and Technology, 7 (4): 13-35.

Kadkhodaie, A., Hosseinzadeh, S., Mosaddegh, H., Kadkhodaie, R., 2019. Pore throat size characterization of carbonate reservoirs by integrating core data, well logs and seismic attributes: Geopersia, 9 (2): 395-410.

Kadkhodaie, A., Rafiei, B., Yosefpour, M., and Khodabakhsh, S., 2011. A committee machine approach for predicting permeability from well log data: a case study from a heterogeneous carbonate reservoir, Balal oil Field, Persian Gulf: Geopersia, 1(2): 1-10.

Kazemi, M., and Takbiri-Borujeni, A., 2016. Flow of Gases in Organic Nanoscale Channels: A Boundary-Driven Molecular Simulation Study: Energy & Fuels, v. 30, no. 10, p. 8156-8163.

Khosravi, V., Mahmood, S. M., Sharifigaliuk, H., and Zivar, D., 2022. A systematic study of Smart Water technology in improving the reservoir recovery performance: Journal of Petroleum Science and Engineering, 216: 110800.

Klinkenberg, L. J., 1941. The Permeability Of Porous Media To Liquids And Gases: Drilling and Production Practice, p. 200-213.

Lei, X., Yao, Y., Sun, X., Wen, Z., Ma, Y., 2022. Permeability change with respect to different hydrate saturation in clayey-silty sediments: Energy, 254: 124417.

Li, S., Dong, M., and Li, Z., 2009. Measurement and revised interpretation of gas flow behavior in tight reservoir cores: Journal of Petroleum Science and Engineering, 65 (1): 81-88.

Martin, A. Z., 2001. Late Permian to Holocene Paleofacies Evolution of the Arabian Plate and its Hydrocarbon Occurrences: GeoArabia, 6 (3): 445-504.

Mazaheri-Johari, M., and Ghasemi-Nejad, E., 2017. Paleoenvironment, Biostratigraphy and Sequence stratigraphic studies of the Permian-Triassic boundrary of the offshore Persian Gulf, Iran: using an integrated approach: Geopersia, 7 (1): 35-54.

McPhee, C., Reed, J., and Zubizarreta, I., 2015. Chapter 5 - Routine Core Analysis, in McPhee, C., Reed, J., and Zubizarreta, I., eds., Developments in Petroleum Science, Volume 64, Elsevier, 181-268.

Mehrabi, H., Bahrehvar, M., Rahimpour-Bonab, H., 2021. Porosity evolution in sequence stratigraphic framework: a case from Cretaceous carbonate reservoir in the Persian Gulf, southern Iran: Journal of Petroleum Science and Engineering, 196: 107699.

Mehrabi, H., Dahaghin, M. H., Ahmadi, Y., 2019. Integrated reservoir rock-typing, hydraulic flow units and electrofacies determination in sequence stratigraphic framework of the Permian–Triassic reservoirs in the central Persian Gulf: Applied Sedimentology, 7 (14): 71-84.

Moradpour, M., Honarmand, J., Monibi, S., Samani, N., Nemati, M., Khodaei, N., Rahimiyan, M. F.-e., 2010. Geological Reservoir Study of the Dalan and Kangan Formations in one of the Gas Field, Persian Gulf: Research Institute of Petroleum Industry.

Nazari Moghaddam, R., Jamiolahmady, M., 2016. Fluid transport in shale gas reservoirs: Simultaneous effects of stress and slippage on matrix permeability: International Journal of Coal Geology, 163: 87-99.

Rahimpour-Bonab, H., Esrafili-Dizaji, B., Tavakoli, V., 2010. Dolomitization and Anhydrite Precipitation in Permo-Triassic Carbonates at the South Pars Gasfield, Offshore Iran: Controls on Reservoir Quality: Journal of Petroleum Geology, v. 33.

Rastegarnia, M., and Kadkhodaie-Ilkhchi, A., 2013. Permeability estimation from the joint use of stoneley wave velocity and support vector machine neural networks: a case study of the Cheshmeh Khush Field, South Iran: Geopersia, 3 (2): 87-97.

Rushing, J. A., Newsham, K. E., Lasswell, P. M., Cox, J. C., and Blasingame, T. A., 2004. Klinkenerg-Corrected Permeability Measurements in Tight Gas Sands: Steady-State Versus Unsteady-State Techniques.

Sfidari, E., Amini, A., Kadkhodaie, A., Ahmadi, B., 2012. Electrofacies clustering and a hybrid intelligent based method for porosity and permeability prediction in the South Pars Gas Field, Persian Gulf: Geopersia, 2 (2): 11-23.

Sharifi Galiuk, H., Aloki Bakhtiari, H., Behin, R., Esfahani, M. R., 2012. X-Ray in-situ saturation monitoring, an aid to study relative permeability in water-wet carbonate rocks: Geopersia, 2 (1): 55-66.

Sharifigaliuk, H., Mahmood, S. M., Zoveidavianpoor, M., Zivar, D., Ayobami Afolabi, F., 2023. Experimental and Modeling Study of Water Imbibition and Flowback in Shale: Prediction of Relative Permeability and Capillary Pressure Curves: Energy & Fuels, 37 (16): 11928-11941.

Szabo, F., and Kheradpir, A., 1978. Permian and Triassic Stratigraphy, Zagros Basin, South-West Iran: Journal of Petroleum Geology, 1 (2): 57-82.

Tanikawa, W., Shimamoto, T., 2009. Comparison of Klinkenberg-corrected gas permeability and water permeability in sedimentary rocks: International Journal of Rock Mechanics and Mining Sciences, 46 (2): 229-238.

Tavakoli, V., 2021. Permeability's response to dolomitization, clues from Permian–Triassic reservoirs of the central Persian Gulf: Marine and Petroleum Geology, 123: 104723.

Tavakoli, V., Rahimpour-Bonab, H., Esrafili-Dizaji, B., 2011. Diagenetic controlled reservoir quality of South Pars gas field, an integrated approach: Comptes Rendus Geoscience, 343 (1): 55-71.

Tavoosi Iraj, P., Mehrabi, H., Rahimpour-Bonab, H., Ranjbar-Karami, R., 2021. Quantitative analysis of geological attributes for reservoir heterogeneity assessment in carbonate sequences; a case from Permian–Triassic reservoirs of the Persian Gulf: Journal of Petroleum Science and Engineering, 200: 108356.

Wojnarowski, P., Czarnota, R., Janiga, D., Stopa, J., 2018. Novel liquid-gas corrected permeability correlation for dolomite formation: International Journal of Rock Mechanics and Mining Sciences, 112: 11-15.